

Electron-impact-induced K plus M shell ionization in solid targets of medium- Z elements studied by means of high-resolution x-ray spectroscopy

T. Ludziejewski,* P. Rymuza, and Z. Sujkowski
Sołtan Institute for Nuclear Studies, 05-400 Świerk, Poland

G. Borchert
Institut für Kernphysik, Forschungszentrum Jülich, D-5170 Jülich, Germany

J.-Cl. Dousse and Ch. Rhême
Physics Department, University of Fribourg, CH-1700 Fribourg, Switzerland

M. Polasik
Faculty of Chemistry, Nicholas Copernicus University, 87-100 Toruń, Poland
 (Received 18 December 1995)

The $K\beta_2$ x-ray spectra of zirconium, niobium, molybdenum, and palladium bombarded by 150 and 300 keV electrons were measured with a high-resolution transmission curved crystal spectrometer. Multiconfiguration Dirac-Fock calculations were used for the decomposition of the experimental spectra into the $K\beta_2M^0$ (diagram) and $K\beta_2M^1$ (satellite) components. The probabilities of energy dependent (direct Coulomb and two-step) processes were estimated from the differences in the satellite line yields for electrons and photons. The satellite yields are found to be considerably enhanced in comparison with those for the proton-induced ionization recently measured and analyzed in the same way [T. Ludziejewski *et al.*, Phys. Rev. A **52**, 2791 (1995)]. This result indicates the importance of multielectron effects in the K plus M shell ionization by energetic projectiles. [S1050-2947(96)03606-2]

PACS number(s): 32.30.Rj, 32.70.Jz, 34.50.Fa, 34.80.Dp

I. INTRODUCTION

The multiple ionization of ions and atoms accompanying the electron impact has been studied in the past mostly by charge collection methods. In a series of experiments absolute cross sections for various target species, atoms, and multiply charged ions were investigated [1–8]. It has been found that multiple ionization is in most cases dominated by the indirect mechanisms of multiple vacancy production [9–12]. These mechanisms are the ionization following a cascading radiative, Auger, or Coster-Kronig transition.

In general, it is difficult to sort out the different individual contributions to the multiple ionization of atoms or ions. Information about direct double ionization inferred from charge state analysis or time of flight spectroscopy is, therefore, limited to the cases where other (indirect) processes are not possible. This situation is achievable either for few electron (He, He-like) targets, or for ionization by electron impact at energies below the subvalence shell threshold.

In the present study we propose an alternative method, in which the K plus M shell ionization by electron impact is studied by means of high-resolution x-ray diffraction spectroscopy. This technique has been widely exploited by us before, for the determination of multiple K plus L , or K plus M shell ionization induced by energetic ions or photons [13–23]. In these measurements, multiplet structures were ob-

served in which the individual (satellite) lines correspond to the transitions with a different number of additional L or M shell holes.

The net energy shift of the K x rays, resulting from the reduced screening of the electron involved in the transition, is sufficient for mid- Z elements to resolve the L shell satellites from the $K\alpha$ or $K\beta_{1,3}$ diagram transitions. For these transitions the energy shifts due to an additional M shell hole are usually smaller than the natural linewidths and cause only a broadening and an energy shift of the diagram or L satellite lines. However, in the case of the $K\beta_2$ transitions, i.e., the transitions involving electrons from the N shell, the energy shift of $K\beta_2M$ satellites is larger than the natural linewidth and these satellites can be observed as well separated lines. Due to the short lifetime of the K shell hole, as compared to the L , M , or higher shells, the number of M shell holes present at the moment of the K x-ray emission nearly corresponds to that created initially in the collision. The slow (in the K shell scale) rearrangement processes, leading to a change of the total number of M shell holes prior to the K x-ray emission, can be accounted for by a simple statistical scaling procedure. Therefore the direct M shell ionization probabilities accompanying the removal of the K shell electrons (i.e., $\sigma_{K,M}/\sigma_K$) can be determined from the measured relative intensities of the satellite and diagram lines. This “satellite” method has been used earlier by us to measure the M shell ionization probabilities in “near central” collisions of fast α particles and protons with Zr, Mo, and Pd targets [14–16,22,23]. Likewise, the method can be applied to determine the relative cross sections of the mul-

*Present address: Gesellschaft für Schwerionenforschung D-64220 Darmstadt, Germany. Electronic address: T.Ludziejewski@gsi.de

multiple inner shell ionization by electrons selectively and for a wide range of bombarding energies.

The theoretical treatment of multiple direct ionization by electrons has not been developed beyond the classical binary encounter approximation (BEA) of Gryziński [24]. While this fully classical theory can still be useful for the discussion of the single total ionization cross sections (BEA1), in the case of the cross sections for double ionization (BEA2) the results in many cases have to be multiplied by a scaling factor 10^{-1} – 10^{-2} [1,2].

On the other hand, quantum mechanical calculations of the direct double ionization are extremely difficult due to the presence of four charged particles in the exit channel interacting with each other via the Coulomb potential. Therefore, from the theoretical point of view, direct multiple ionization by electron impact can yield interesting information about the correlation effects [25] and can be treated as a sensitive test of the importance of the many electron interactions which are neglected in the independent particle model. From the point of view of possible applications the direct multiple ionization cross sections can be important for the evaluation of the charge state evolution in the electron beam ion source (EBIS) [26]. In this context experimental, as well as theoretical, studies of direct double ionization by electrons are of great interest.

The subject of the direct multiple ionization by electron impact studied by means of high-resolution x-ray or Auger electron spectroscopy has been addressed by several authors. In an early work of Carlson *et al.* [27], the K plus L shell ionization of neon and L plus M shell ionization of argon were investigated as a function of the energy of the impact electrons. The cross sections for double relative to single ionization were discussed in terms of the sudden approximation (SA) model, in which the single mechanism responsible for the double vacancy production is the shake process. It was found that the ratio of double to single ionization is independent of the energy of the incident electrons at higher energies. However, at low energies the probabilities for double (K plus L , or L plus M) ionization can exceed the high-energy limit. This low-energy excess was attributed to the admixture of direct Coulomb ionization (DI) by the electron impact. The same conclusion was drawn from measurements of the Auger satellites induced by photon, electron [28], and proton beams [29]. These measurements indicated that the K plus L shell ionization of Ne is independent of the excitation mode and reasonably well reproduced by the sudden approximation calculations of shake effects except for low-energy protons, where direct Coulomb ionization and electron capture start to play a role.

In a systematic study of the energy dependence of the $I(KL^n)/I(KL^0)$ satellite line intensity ratio carried out for a variety of elements ($9 \leq Z \leq 29$) [30] up to two satellites accompanying the K shell ionization by electrons have been observed. Similarly, it was concluded that besides the shake effect, energy dependent processes (DI, and/or secondary ionization) can also play an important role in multiple K plus L shell ionization.

The present work concentrates on the double (K plus M shell) ionization processes induced by 150 keV and 300 keV electron beams in Zr, Nb, Mo, and Pd targets. The $K\beta_2M^1$ satellites were measured using an on-line bent crystal diffrac-

tion spectrometer operated in the modified DuMond slit geometry. The spectra were analyzed with the help of extensive multiconfiguration Dirac-Fock calculations.

Similar experiments have been recently carried out for Zr, Mo, and Pd targets where the K plus M shell ionization was induced by energetic proton beams and photons [22]. In this paper a comparison is given between the direct M shell ionization probabilities accompanying the K shell ionization by protons and electrons. The experimental conditions did not allow for measurements of the $K\beta_2$ satellite spectra for electron velocities matching those for protons. In spite of this limitation such comparison seems to be instructive.

The direct Coulomb ionization probabilities by charged particles were determined from the differences in the $K\beta_2$ satellite yields in the charged particle and photoinduced spectra. The relative importance of shake and energy dependent processes has been verified for the high-energy electrons. To the authors' knowledge there are no published experimental data concerning direct M shell ionization probabilities by electron impact for mid- Z targets.

II. EXPERIMENT

The experiments were performed at the Sołtan Institute for Nuclear Studies in Świerk near Warsaw. The electron beams were accelerated by the EAK-400 facility to energies of 150 ± 10 keV and 300 ± 10 keV and focused to circular beam spots with a diameter of 2 mm. The beam currents were varied from several tens to several hundreds of μ A depending on the investigated target. Natural, 5 and 15 μ m Zr, 10 μ m Nb, 5.9 and 10 μ m Mo, and 8 μ m thick Pd self-supporting foils, and targets mounted on a water cooled carbon backing were used.

The x rays produced by the electron beams were measured with an in-beam bent crystal spectrometer operated in the modified DuMond slit geometry. A schematic diagram of the experimental setup is presented in Fig. 1. In this design two plates of tantalum, forming a 0.2 mm narrow slit, are placed in front of the target on the focal circle. The slit acts as the effective source of radiation. This geometry permits one to avoid the line shape problems caused by the thermal deformation or displacement of the target. The target itself is placed at an angle $\Phi = 40^\circ - 50^\circ$ to the beamline which is perpendicular to the plane (x, y) of the spectrometer. Three remote-controlled stepping motors are used to align and optimize the target and slit positions. They permit one to rotate the target around the y axis, to displace it transversely (y direction), and to move the slit in the target-crystal direction (x direction).

The diffraction spectrometer used in this experiment was constructed in KFA-Jülich for high-resolution measurements of low-energy γ rays and x rays of mid- Z and heavy elements. For the present study the maximum Bragg angle of the spectrometer was extended to 8.1° in order to allow the measurements of the $K\beta$ x rays of elements with $Z \geq 40$. The (110) planes of a 3.5 mm thick quartz crystal plate bent to the radius of 4.64 m were used for the reflection of x rays. The active reflecting area was 24 cm². The Bragg angles θ were measured with an interferometric system with an accuracy better than 0.01 arc sec. The detailed description of the instrument can be found elsewhere [31,32]. For the detection

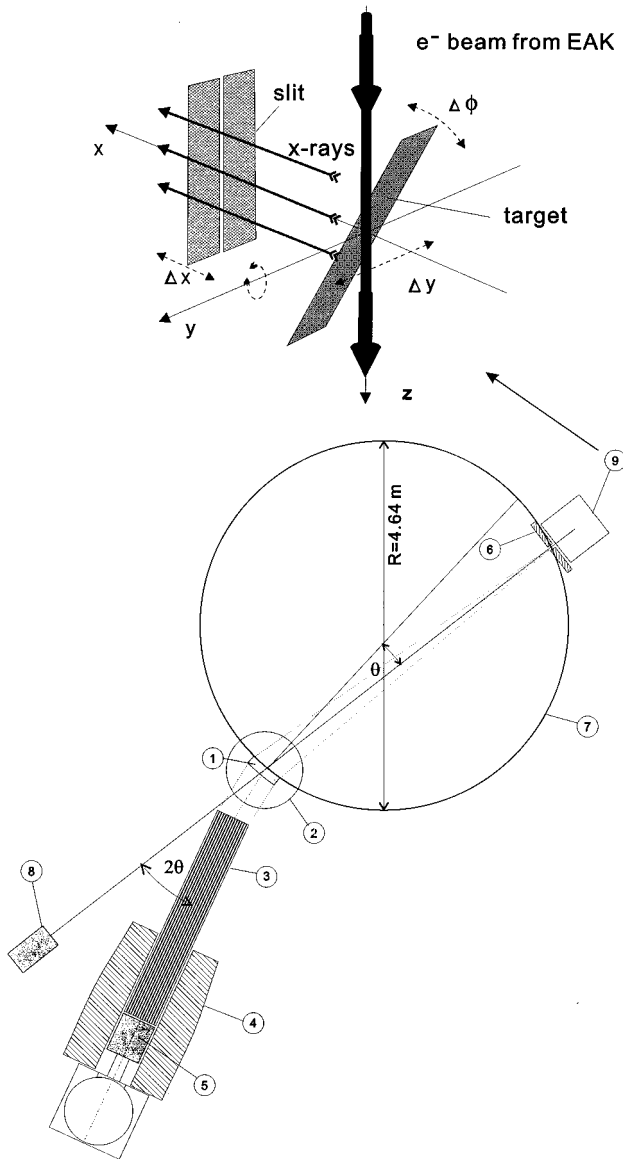


FIG. 1. The schematic view of the crystal spectrometer: (1) quartz crystal, (2) interferometric system, (3) collimator, (4) Pb shield, (5) HP-Ge detector, (6) slit, (7) focal circle, (8) Si-Li monitoring detector, and (9) target chamber. The details of the target-slit arrangement are shown in the upper part of the figure.

of the diffracted x rays a HP-Ge detector 6 cm in diameter surrounded by a Pb shield was employed.

The beam intensity was monitored by an 80 mm^3 Si(Li) detector placed at 0° behind the quartz crystal and viewing the target through the slit and the quartz crystal. The selected regions in the monitoring detector, corresponding to the K x rays of interest and to the background (stemming mainly from the electron bremsstrahlung), were used to ensure that all points measured in preset count mode correspond to equal numbers of K shell ionization events. All spectra were measured in the first order of reflection, and in several scannings, in order to survey the stability and reproducibility of the measurements. In addition, for each target element and each energy, at least two independent measurements were performed with either different target thicknesses or different target mounting (self-supporting targets or targets on a carbon backing). The spectra were energetically autocalibrated

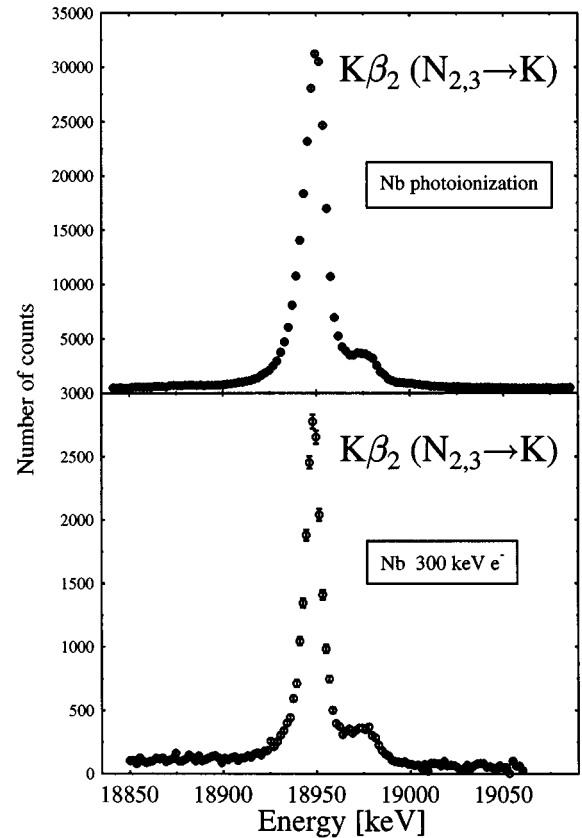


FIG. 2. Crystal spectrometer x-ray spectrum of Nb induced by photoionization (upper part) and 300 keV electron impact (lower part).

using the tabulated energies of the $K\beta_2$ transitions [33] and the known energy-angle characteristic of the interferometer.

The measurements of the photoinduced $K\beta_2$ spectra were performed at Fribourg University with the use of a similar bent crystal spectrometer installation. The photoionization data for Zr and Mo were taken from recent work [22] while the data for Nb were measured in this work using the same technique as that described in Ref. [22]. In addition, as a consistency check of the data of Ref. [22], the $K\beta_2$ spectra of Pd were remeasured for a thinner ($8 \mu\text{m}$) target. For illustration, the crystal spectrometer spectra of Nb induced by photons and 300 keV electron beam are shown in Fig. 2.

III. DATA ANALYSIS AND RESULTS

The method of data analysis applied in the present study is essentially the same as that used in [22]. Therefore the absorption corrections, multiconfiguration Dirac-Fock (MCDF) calculations of the x-ray profiles, fitting procedure, and corrections for electron rearrangement will be only briefly described here.

For medium-heavy elements such as Zr, Nb, Mo, and Pd the K absorption edges partially overlap with the $K\beta_2$ satellite region. As a consequence the measured spectra have to be corrected for the steplike increase of the self-absorption in the target. The change of the self-absorption as a function of the photon energy for photoinduced spectra was deduced by measuring the transmission of the x rays through the Zr, Nb,

Mo, and Pd foils. In these measurements the spectrometer was used as a monochromator. The spectral intensity distribution of the x-ray tube was used to calculate the variation of the target activity as a function of the penetration depth of the ionizing radiation. In contrast, for the correction of the electron-induced spectra, the theoretical absorption edge profiles (calculated as a convolution of the known natural width of the K shell hole states with the experimentally determined instrumental resolution of the spectrometer) were used. The electron-induced ionization was assumed to be constant over the entire target thickness. This assumption is reasonable since much thinner (5–15 μm) targets were used for e^- -induced spectra.

The M shell ionization probabilities accompanying the K shell electron ejection by e^- or photon impact can be determined from the formula

$$p_M^{\text{tot}} = 18 \frac{I_M}{(18 + I_M)}. \quad (1)$$

This formula, which was used in our previous study [22], was also employed in the present investigation for a consistent comparison between the results of the two experiments. In Eq. (1) p_M^{tot} is the total M shell ionization probability, and I_M is the satellite to diagram line intensity ratio corrected for the self-absorption and the rearrangement processes. The quantity I_M can also be interpreted as the ratio of the cross sections for the production of one K and one M to one K and zero M shell holes:

$$I_M = \frac{\sigma_{1K,1M}}{\sigma_{1K,0M}}. \quad (2)$$

The x-ray transition profile measured with the diffraction spectrometer has in general a complicated structure. Since the instrumental resolution is comparable to the natural line-width, a transition between two states should in general be represented as the convolution of a Lorentzian and a Gaussian. The folding of the two functions results in a so-called Voigt profile, for which the natural line is described by the Lorentzian shape, while the instrumental resolution is represented by the Gaussian shape. In the case of multiply ionized atoms and/or atoms with open valence shells, the x-ray profile is still more complicated, since many states differing in total angular momentum (and, therefore, energy) can represent a particular electron configuration. As a consequence, the resulting shape of the x-ray line profile should be constructed by summing up all the possible transitions with the weights corresponding to their transition probabilities. In the present work the energies and transition probabilities of the individual (diagram and satellite) components were calculated by means of the multiconfiguration Dirac-Fock computer code GRASP [34]. The MCDF calculations were performed using the modified special average level (MSAL) version [35] which has proved to be an efficient and adequate method for the description of the x-ray transitions in multiply ionized atoms. In the MCDF calculations the $[\text{Kr}] 4d^0 5s^2$, $[\text{Kr}] 4d_{3/2}^4 4d_{5/2}^0 5s^2$, and $[\text{Kr}] 4d^{10}$ simplified closed valence shell ground-state configurations were chosen for Nb, Mo, and Pd, respectively, while for Zr the calculations for the realistic $[\text{Kr}] 4d^2 5s^2$ open valence shell ground-state

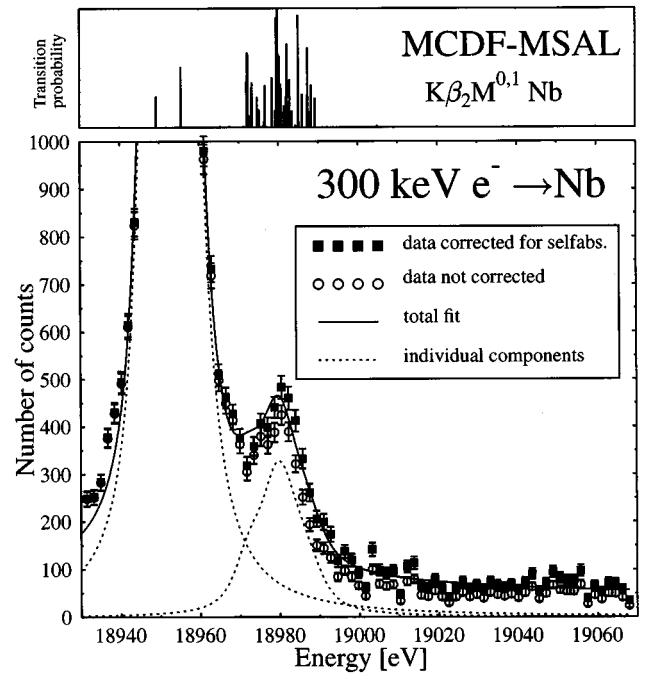


FIG. 3. Expanded part of the $K\beta_2$ spectrum of Nb (see Fig. 2) induced by 300 keV electrons. The empty markers represent raw data, while the full squares show the spectrum corrected for the self-absorption of the x rays in the target. The overall shape of the fitted spectrum is represented by the solid line, whereas the dotted lines correspond to the individual profiles of the $K\beta_2M^0$ and $K\beta_2M^1$ components constructed on the basis of MCDF calculations. In addition the results of the MCDF calculations are represented schematically as a stick plot in the upper inset.

configuration were carried out. The numerical method used for the decomposition of the experimental spectra into the $K\beta_2M^i$ ($i=0,1$) components was based on the Lavenberg-Marquardt nonlinear least-squares fitting routine, an efficient convolution method exploiting fast Fourier transform.

In Fig. 3, as an example, an expanded part of the $K\beta_2$ satellite region of Nb bombarded by 300 keV electrons is presented. The effect of the self-absorption corrections and the results of the fitting procedure are visualized. The fitted profiles agree fairly well with the experimental spectrum in spite of the fact that the rearrangement effects leading to the redistribution of the M subshell holes have not been taken into account in the theoretical construction of the $K\beta_2M^1$ line profile. The energies and relative intensities of the diagram and satellite components calculated using the MSAL version of MCDF program GRASP are presented schematically in the upper part of Fig. 3.

The satellite yields extracted from the fit reflect the hole distribution in the target atoms at the moment of the K x-ray emission and not the initial hole distribution induced by the interaction with the projectile. The latter can be estimated, however, using a simple, statistical scaling procedure [22]. As long as the total number of M shell holes is taken into account, the radiative, Auger, or super-Coster-Kronig rearrangement transitions do not change considerably the initial vacancy configuration. This is a consequence of the short lifetime of the K shell hole as compared to the radiative and

TABLE I. The M shell ionization probabilities deduced from the $K\beta_2M^1$ satellites of Zr, Nb, Mo, and Pd, induced by photoionization and by proton and electron impact ionization. Errors are listed in parentheses. The heading ‘‘low E ’’ means the low-energy regime of the operation of the x-ray tube, while ‘‘high E ’’ stands for the high-energy regime (for details see Ref. [22]). Data marked by † were taken from [22].

	Zr	Nb	Mo	Pd
Photoion.	7.58 [†]	9.11	8.20 [†]	2.64
low E	(0.38)	(0.24)	(0.38)	(0.22)
Photoion.	8.39 [†]	9.68	8.60 [†]	2.98
high E	(0.35)	(0.21)	(0.36)	(0.20)
16 MeV p^\dagger	9.25		9.45	4.12
	(0.62)		(0.36)	(0.30)
25 MeV p^\dagger	9.16		8.52	3.17
	(0.36)		(0.46)	(0.33)
45 MeV p^\dagger	9.76		8.10	3.10
	(0.30)		(0.33)	(0.34)
150 keV e^-	13.5	13.4	11.7	7.7
	(1.6)	(1.2)	(0.7)	(0.6)
300 keV e^-	12.9	13.8	12.9	8.0
	(1.2)	(1.0)	(0.7)	(0.66)
Shake (SA calc.)	3.428	3.001	2.730	1.831

nonradiative Auger or super-Coster-Kronig transitions.

The average M shell ionization probabilities accompanying the removal of a K shell electron of Zr, Nb, Mo, and Pd in the photoionization process or by proton or electron impact are listed in Table I and plotted in Fig. 4. The entries were calculated according to Eq. (1), with the underlying assumption that the yields in the $K\beta_2$ satellite region are due only to the simultaneous (K plus M) shell ionization. Since within the statistical errors no differences were found for various target thicknesses (or target mounting conditions) the data for electrons listed in Table I represent the values averaged over several independent measurements. The data for protons, as well as the photoionization data for Zr and Mo, were taken from our recent work [22]. The errors listed in parentheses are due only to the fitting procedure and do not include the systematic errors due to the assumed line shape model, the self-absorption corrections, or the uncertainties due to the rearrangement procedure.

In addition, the predictions of the sudden approximation calculations of shake-off plus shake-up processes are included in Table I and plotted in Fig. 4(a). In the sudden approximation model the probability for either exciting (shake up) or ionizing (shake off) an electron from a given atomic orbital is calculated assuming instantaneous change of the central potential. This model leads to simple expressions (see, e.g., [22,36]) in which the shake amplitude is proportional to the overlap between the initial and final wave functions. In the calculations whose results are listed in Table I we used the self-consistent Dirac-Fock wave functions from the GRASP program.

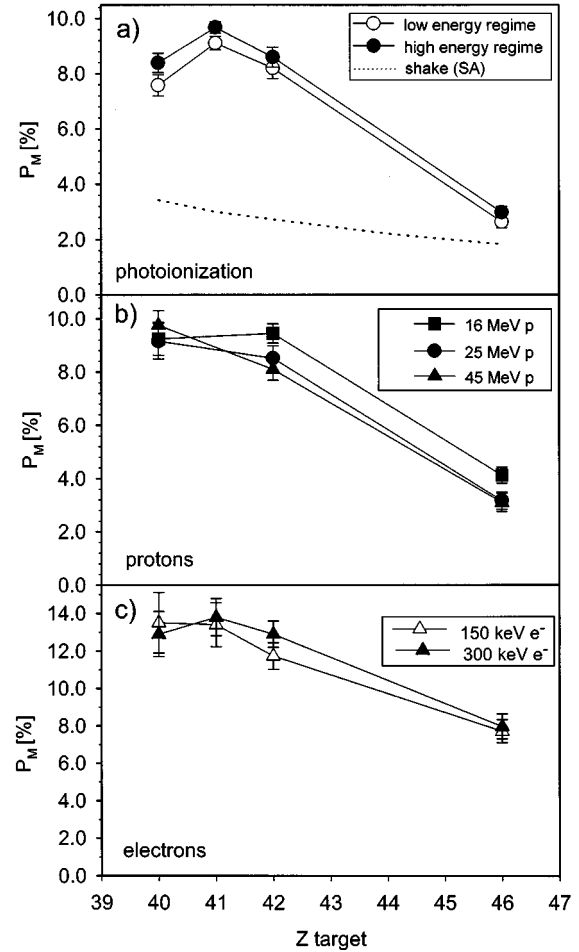


FIG. 4. Total M shell ionization probabilities induced by (a) photons, (b) 16, 25, and 45 MeV protons (data taken from our recent work [22]), and (c) 150 and 300 keV electrons. Dotted line in (a): results of the sudden approximation calculations of the shake probabilities.

IV. DISCUSSION

A. Total yields of the $K\beta_2$ satellite lines

The key parameter deciding whether the SA is applicable for the case of the shake process following the ejection of an electron from the atom is the velocity of this primary electron. According to [37], the sudden approximation is valid when the energy transferred to the ejected electron (E_{ph}) exceeds significantly the ionization threshold (E_{bind}) for the shake-off electron. An empirical criterion of the applicability of the SA found for photoionization [38] and electron impact ionization [39] is that $E_{ph} > 3E_{bind}$.

From the comparison of the existing experimental data with the SA calculations it follows that the theory does provide a good estimation of the shake probabilities as long as the process is sufficiently violent and involves electrons from different shells. However, the model fails for the shake processes when the shaken electron belongs to the same shell in which the initial hole was created, that is, e.g., for the shake off accompanying nuclear electron capture or the double photoionization of helium.

The photoionization data shown in Fig. 4 were measured by means of an x-ray tube. The energy distribution of the radiation emitted by the x-ray tube was measured with a semiconductor detector. The average photoelectron energies determined from this direct measurement are 30 and 10 times larger than the ionization threshold for the “high-energy regime” and the “low-energy regime,” respectively. Thus the application of the SA for the description of the present data seems to be well justified.

A comparison of the SA calculations with the experimental results for photoionization [see Fig. 4(a)] shows a considerable (more than a factor of 3 for Nb) enhancement of the satellite line intensities as compared to the SA theory. Further, the experimental probabilities show a nonmonotonic dependence of the total p_M as a function of the target atomic number. The new data for Nb confirmed this trend, pointed out already by us in Ref. [22]. Although the shake process should play a decisive role in the K plus M shell ionization by photon impact, the observed target atomic number dependence does not follow the SA calculations, which predict decreasing ionization probability as a function of the target atomic number. Similar target atomic number dependence is also observed for the K plus M shell ionization by protons [Fig. 4(b)] and electrons [Fig. 4(c)]. In these cases, however, the Coulomb ionization processes additionally come into play.

The properties described above suggest that there is an additional mechanism responsible for the enhancement of the $K\beta_2$ satellites. It was postulated [22] that a major part of the discrepancy between the experiment and the SA theory is due to solid-state effects relaxing the quadrupole character of the $K\beta_4$ ($4d_{3/2,5/2} \rightarrow 1s$) transitions. Within the convoluted natural linewidth and the instrumental resolution of diffraction spectrometers, these transitions overlap with the average energy of the $K\beta_2M^1$ satellite transitions for the atomic number range $40 \leq Z \leq 46$. In isolated atoms the contribution of the quadrupole $K\beta_4$ transitions should remain small [$I(K\beta_4)/I(K\beta_2) \approx 1.1 \times 10^{-3}$ for Mo [40]]. In a solid, however, the band character of the $4d$ subshell and the mixing of the p and d states may bring a sharp increase of their intensity. Support for this conclusion can also be found in the recent investigation of the x-ray transitions from the valence states to the $1s$ or $2s$ levels in metallic Mo and several Mo compounds [41].

It is worth noting here that one can determine the contribution of the solid-state effect to the total $K\beta_2$ satellite intensity, or at least an upper limit thereof, from a precise measurement of the $K\beta_2M^2$ satellite yield. Assuming that the production of the two M shell holes is uncorrelated, the intensity of the $K\beta_4$ transition in a solid can be determined from the difference of the measured $K\beta_2M^1$ satellite intensity and that calculated using the p_M value deduced from the $K\beta_2M^2$ line intensity and the binomial distribution. In fact, the second ($K\beta_2M^2$) satellite was observed in the photoinduced $K\beta_2$ spectrum of Nb. However, the large self-absorption corrections for the relatively thick target used, as well as nonoptimal background rejection conditions, have resulted in too poor an accuracy to carry out a reliable quantitative analysis. Experiments aiming at such an accuracy are in progress.

From the inspection of Fig. 4(a) one can also conclude that there is a systematic difference in the total p_M for the high- and low-energy regimes of the photoionization. For each target the ionization probability is systematically higher for larger average energy of the impinging photons. The observed differences cannot be explained by the influence of the solid-state effect or the “shake” effect in the sudden approximation limit. The question then remains what type of energy dependent process accounts for the observed differences in the photoionization data for the two distinct average energies of the impinging photons.

Further, the comparison of K plus M shell ionization induced by protons and electrons shown in Figs. 4(b) and 4(c) reveals that the intensity ratios $I_{K,M}/I_K$ are noticeably larger for electrons than for protons. As indicated earlier, instead of the shake processes and the solid-state effect the Coulomb interaction among the charged projectile and the bound inner shell electrons possibly leads to additional K plus M shell ionization.

Various scenarios have been proposed in the literature to describe the double ionization process by charged particles. Retaining the classical picture, at high energies, apart from the shake processes mentioned earlier, two-step (TS) ionization can play an important role (see, e.g., [42]). For example, following a single interaction between the projectile and the target electron, a second bound electron can be ionized in a subsequent collision with the projectile (the classical analogue of direct Coulomb ionization, also called the TS-2 process). This mechanism is to be contrasted with the process in which the δ electron ejected in the primary collision interacts with the second bound electron and produces double ionization (TS-1). The latter process is expected to dominate over TS-2 in the limit of high projectile velocities. It is worth noting here that TS-2 is possible only for charged particle impact, while TS-1 can also be an important channel in photoionization. In the above picture we assumed that electrons are distinguishable, and therefore the exchange term is negligible. This is the case for the incident and ejected electrons, but not always true for the two inner shell electrons ejected simultaneously with similar velocities from the atom and sharing the same region in phase space.

B. Energy dependent processes

In order to elucidate in more detail the role of direct Coulomb and TS-1 processes by electron impact we have subtracted the relative intensities of the $K\beta_2M^1$ satellites for photons from those for charged particles. The resulting yields can be attributed to the direct Coulomb M shell ionization probability p_M^{DI} accompanying the K shell ionization if one assumes that the TS-1 processes are the same for charged particle and photon impact. This assumption is not fully satisfied in our case, due to the differences in the velocity distributions of the ejected electrons for collisions with electrons, protons, and photons. These are particularly large for photoionization and charged particle impact. However, the procedure allows one to get rid of the solid-state and shake effects in the SA limit, since these effects are independent of the ionizing agent.

The results for 150 and 300 keV electron impact on Zr, Nb, Mo, and Pd are presented in Fig. 5 together with the

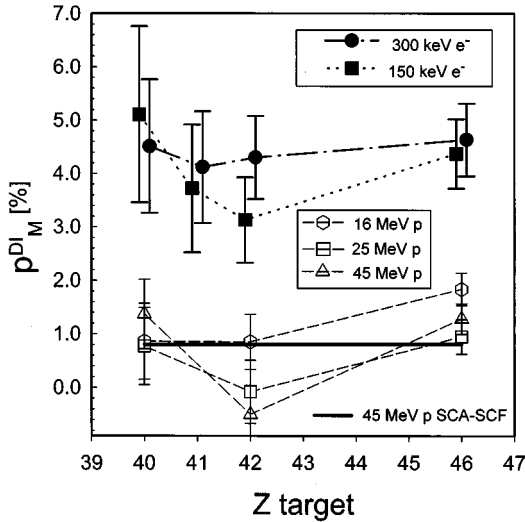


FIG. 5. Probabilities for direct Coulomb plus TS-1 ionization obtained by subtracting from the relative yields of the $K\beta_2M^1$ satellites for charged-particle-induced ionization the corresponding yields for photoionization (measured in the ‘‘high-energy regime’’). Solid curve represents the SCA calculations for 45 MeV protons on Zr, Mo, and Pd.

corresponding results for 16, 25, and 45 MeV protons on Zr, Mo, and Pd taken from Ref. [22]. In addition, relativistic semiclassical approximation (SCA) calculations of the direct Coulomb ionization probabilities for ionization by 45 MeV protons are shown. In the SCA calculations presented in Fig. 5 Dirac-Fock wave functions were used. It has been shown recently [19,23] that the SCA model with realistic wave functions gives good agreement with the experimental inner shell ionization probabilities even for large reduced velocities, for which the same calculations employing hydrogenic-like wave functions fail. The calculations agree reasonably well for protons, suggesting that the TS-2 process plays in this case a major role in the Coulomb ionization.

Several trends may be noted in comparing experimental data for electron and proton impact. For both types of projectiles there is a similar weak dependence of the p_M^{DI} on the target atomic number. The comparison shows, however, a drastically larger p_M^{DI} for electrons than for protons. In addition, within the experimental error bars there is no difference in the p_M^{DI} for the two different energies of the impinging electrons.

These results are rather surprising in view of the fact that the direct Coulomb ionization in the high-energy limit varies with velocity of the projectile v approximately as $\ln(v^2)/v^2$, and the cross sections for protons and electrons become equal for a given v at sufficiently large but nonrelativistic velocities.

For the 45 MeV protons the velocity is equal to 0.30 of that of light, while for 150 and 300 keV electrons the velocities are $0.63c$ and $0.78c$, respectively. Hence, provided that v is sufficiently large but nonrelativistic, the corresponding cross sections should be $\sigma_{\text{DI}}(p) > \sigma_{\text{DI}}(150 \text{ keV } e^-) > \sigma_{\text{DI}}(300 \text{ keV } e^-)$.

To discuss in more detail the mechanisms of ionization responsible for the observed differences in the electron and proton experiments, we have to investigate which effects can

influence the observed satellite line intensities. The first process is the alignment induced by charged particles, which may lead to an anisotropy in the angular distribution of the satellite x rays; the second one is related to the relativistic corrections that modify the ionization amplitude.

In the ionization of inner atomic subshells with the total angular momentum $j > 1/2$ by a beam of charged particles, the probability of ionization may have different values for different moduli of the projection of j on the quantization axis. This means that while no anisotropy can be observed for the diagram K x rays (for which there is only one possible quantum number, $|m| = 1/2$), the angular distribution can be anisotropic for the satellite $K\beta_2M^1$ transitions, for which there exist many possible initial states characterized by angular momentum $j > 1/2$. The so-called alignment of atomic subshells has been studied theoretically for electron impact ionization [43] as well as for ion-atom collisions [44]. It has been found that while in general non-negligible, the charged-particle-induced alignment tends to zero for reduced velocities $v_{\text{red}} \gg 1$. Further, describing the alignment of the atom with a K and an M shell hole, one has to take into account that the spectator vacancies couple to many different possible total angular momentum values J . In this case the coefficients of anisotropy which are proportional to $(-1)^{j_{\text{init}} + j_{\text{final}} + 1}$ add with opposite signs, reducing the effective value of the alignment. It is worth noting, in addition, that the proton-induced $K\beta_2M^1$ spectra were measured for the ‘‘magic angle’’ 55° for which the probability for photon emission does not depend on the alignment tensor component $\mathcal{A}_{2,0}$. We can state, therefore, that the anisotropy effects cannot be responsible for the observed strong differences in proton- and electron-induced $K\beta_2M^1$ satellite yields.

To estimate the role of the relativistic corrections in the M shell ionization of mid- Z targets by 150 and 300 keV electrons (stemming mainly from the magnetic interaction) we exploited the semiempirical calculations of absolute inner shell ionization cross sections developed by Deutsch *et al.* [45]. The model (in the following denoted as D-M) provides absolute cross sections for K , L , and M shell ionization which are in satisfactory agreement with the experimental data in the energy range from threshold up to 10^9 eV and for all elements. In Fig. 6 results of the D-M calculations which take into account relativistic corrections are plotted for the case of Mo from threshold to 5×10^5 keV. Also shown are the results of the nonrelativistic BEA theory and the nonrelativistic semiempirical calculations according to the Lotz formula [46].

The comparison of the calculated M shell cross sections shows a reasonable agreement between the Lotz formula and the BEA model. As can be seen from the comparison of the nonrelativistic BEA or Lotz models and the D-M calculations, the relativistic term in the D-M model starts to play a role at approximately 100 keV. Further, the relativistic corrections change the total σ_M approximately by 20% for 150 keV electrons and at most by 50% for 300 keV electrons. Recalling the earlier mentioned scaling rule $\sigma_M \sim \ln(v^2)/v^2$, we can state that the direct Coulomb ionization cannot be responsible for the observed enhancement of the M shell ionization probability even when we take into account the relativistic corrections.

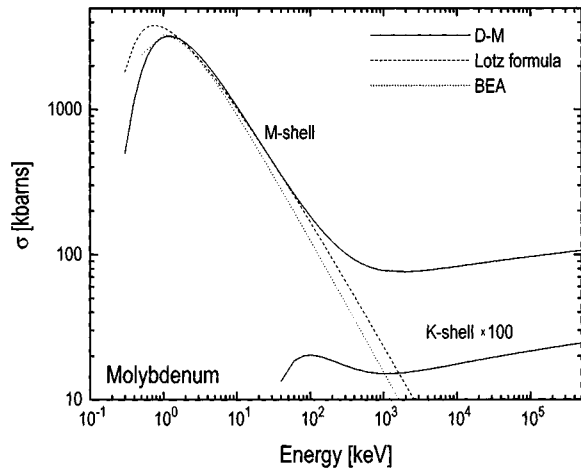


FIG. 6. Total M shell ionization cross sections for molybdenum; solid line: relativistic D-M model; dotted line: nonrelativistic calculations according to the Lotz formula; dashed line: BEA calculations. In addition, D-M calculations of the K shell ionization cross sections are plotted.

The double ionization by charged particles and photons in recent years attracted the attention of both experimental and theoretical physicists due to the fundamental role of many body interactions involved in the process. Particularly interesting were the differences in the high-energy limit of double to single ionization cross section ratios (σ^{++}/σ^+) of helium by charged particles and photons [47], as well as the large differences observed under charge conjugation for (p^+, p^-) and (e^+, e^-) projectiles (see, e.g., [48,49]). It is generally believed that Compton scattering and successive absorption of scattered photons by the second electron as well as ground-state correlations are important factors responsible for the differences in the high-energy limit for photons and charged particles. These processes are, however, of no importance in the case of (K plus M) shell ionization of mid- Z atoms by several keV photons, due to the small Compton scattering cross sections as compared to photoionization cross sections and the weak correlation of the K and M shell electrons. Similarly, the huge differences in the double to single ionization cross section ratios between electrons, positrons, protons, and antiprotons observed for helium were explained in general as being due to correlations. However, no consensus has been reached as to the physical mechanism of correlation. Besides the correlated shake process, the TS-1 is thought to be important for sufficiently large projectile velocities. McGuire [50] and Végh and Burgörfer [42] suggested that the interference between the shake and the TS quantum amplitudes may be responsible for the observed larger double- to single-ionization cross section ratios for electrons with respect to that for protons. This interference may be restricted, however, by the selection rules. The classical trajectory Monte Carlo calculations of Olson [51] show that the effects may be explained without quantum interference and that they are caused by the different reaction kinematics for different types of projectiles. The effects of reaction kinematics, polarization, and screening (antiscreening) are considered to be important only for not too high impact velocities.

In analogy to the double ionization of He we can state that in the case of double K plus M shell ionization of medium-

Z atoms, besides the trivial shake and direct Coulomb interaction (TS-2), there are additional mechanisms which contribute to the ionization amplitude. These are correlation and/or TS-1 processes influencing the σ_{KM}/σ_K cross section ratio. In the case of the photoionization data [see Fig. 4(a)] the TS-1 mechanism manifests itself as a difference between the K plus M to K ionization probability ratio for two distinct energy distributions of the impinging photons. For charged particles, it is possible that the positive and negative interference among TS-1, TS-2, and shake amplitudes in the case of ionization by electrons and protons, respectively, leads to the observed differences in σ_{KM}/σ_K .

It is worth noting here that for the large velocities of electrons and protons discussed in the present paper, an additional scenario of the TS-1 process is possible. In the reversed TS-1 process the scattering of the projectile on the M shell electron can be followed by K shell ionization induced by the scattered electron. The differences in the collision dynamics imposing different upper and lower limits of the momentum transfer for proton and electron impact (the δ electrons are ‘harder’ for 300 keV electrons than for impact of 45 MeV protons) may cause the contribution of the reversed TS-1 process to be larger in the case of electrons.

V. SUMMARY AND CONCLUSIONS

The $K\beta_2$ diagram and satellite transitions have been systematically measured for solid Zr, Nb, Mo, and Pd targets bombarded with 150 and 300 keV electrons. The measurements have been done with the use of a bent crystal diffraction spectrometer. This technique allows one to determine state selective double to single (K plus M to K) cross section ratios for high energies of projectiles, which are difficult to measure for complex atoms with other experimental methods.

Probabilities for the energy dependent M shell ionization processes were obtained by subtracting the satellite to diagram line intensity ratio for photon impact from that for electron impact. These values can be compared with the corresponding results obtained recently for protons. The comparison demonstrates that the probabilities for the energy dependent processes are substantially higher for electrons than for protons.

Various processes leading to the observed enhancement of the satellite to diagram $K\beta_2$ line intensity ratios for electrons are discussed. The discussion leads to the conclusion that in addition to the Coulomb ionization and to the ionization by shake off, the multielectron two-step processes, and possibly interference between TS-2, TS-1, and shake-off effects influence the ionization probabilities significantly.

ACKNOWLEDGMENTS

The authors gratefully acknowledge the assistance of the members of the EAK accelerator staff. One of us (T.L.) wants to express particular thanks for the kind hospitality during his stay at Fribourg University. Partial support for this work was provided by the Polish Committee for Scientific Research (KBN) Grants No. 2 P 302 119 07, No. 2 P 03B 055 09, and No. 115 P03 95 09, and by the Swiss National Science Foundation.

- [1] K. Tinschert, A. Müller, R. A. Phaneuf, G. Hoffman, and E. Salzborn, *J. Phys. B* **22**, 1241 (1989).
- [2] M. Zambra, D. Belic, P. Defrance, and D. J. Yu, *J. Phys. B* **27**, 2383 (1994).
- [3] K. Tinschert, A. Müller, R. Becker, and E. Salzborn, *J. Phys. B* **20**, 1823 (1987).
- [4] M. B. Schach, P. McCallion, K. Okuno, and H. B. Gilbody, *J. Phys. B* **26**, 2393 (1993).
- [5] V. Schmidt, N. Sander, and H. Kutzenmüller, *Phys. Rev. A* **13**, 1743 (1976).
- [6] Ch. Achenbach, A. Müller, E. Salzborn, and R. Becker, *Phys. Rev. Lett.* **26**, 2070 (1983).
- [7] A. Müller and R. Frodl, *Phys. Rev. Lett.* **44**, 29 (1980).
- [8] M. S. Pindzola, D. C. Griffin, C. Bottcher, D. H. Crandall, R. A. Phaneuf, and D. C. Gregory, *Phys. Rev. A* **29**, 1749 (1984).
- [9] M. H. Chen and K. J. Reed, *Phys. Rev. A* **47**, 1874 (1993).
- [10] R. A. Falk, G. H. Dunn, D. C. Griffin, C. Bottcher, D. C. Gregory, D. H. Crandall, and M. S. Pindzola, *Phys. Rev. Lett.* **47**, 494 (1981).
- [11] K. T. LaGutta and Y. Hahn, *Phys. Rev. A* **24**, 2273 (1981).
- [12] D. C. Griffin, C. Bottcher, M. S. Pindzola, S. M. Younger, D. C. Gregory, and D. H. Crandall, *Phys. Rev. A* **29**, 1729 (1984).
- [13] P. Rymuza, Z. Sujkowski, M. Carlen, J.-Cl. Dousse, M. Gasser, J. Kern, B. Perny, and Ch. Rhême, *Z. Phys. D* **14**, 37 (1989).
- [14] M. Carlen, J.-Cl. Dousse, M. Gasser, J. Kern, Ch. Rhême, P. Rymuza, Z. Sujkowski, and D. Trautmann, *Europhys. Lett.* **13**, 231 (1990).
- [15] M. Carlen, J.-Cl. Dousse, M. Gasser, J. Hoszowska, J. Kern, Ch. Rhême, P. Rymuza, and Z. Sujkowski, *Z. Phys. D* **23**, 71 (1992).
- [16] P. Rymuza, T. Ludziejewski, Z. Sujkowski, M. Carlen, J.-Cl. Dousse, M. Gasser, J. Kern, and Ch. Rhême, *Z. Phys. D* **23**, 81 (1992).
- [17] D. F. Anagnostopoulos, G. L. Borchert, D. Gotta, and K. Rashid, *Z. Phys. D* **18**, 139 (1991).
- [18] T. Ludziejewski, J. Hoszowska, P. Rymuza, Z. Sujkowski, D. Anagnostopoulos, G. Borchert, M. Carlen, J.-Cl. Dousse, Ch. Rhême, and A. G. Drentje, *Nucl. Instrum. Methods Phys. Res. Sect. B* **63**, 494 (1992).
- [19] D. F. Anagnostopoulos, G. L. Borchert, and D. Gotta, *J. Phys. B* **25**, 2771 (1992).
- [20] M. W. Carlen, M. Polasik, B. Boschung, J.-Cl. Dousse, M. Gasser, Z. Halabuka, J. Hoszowska, J. Kern, B. Perny, Ch. Rhême, P. Rymuza, and Z. Sujkowski, *Phys. Rev. A* **46**, 3893 (1992).
- [21] M. W. Carlen, B. Boschung, J.-Cl. Dousse, Z. Halabuka, J. Hoszowska, J. Kern, Ch. Rhême, M. Polasik, P. Rymuza, and Z. Sujkowski, *Phys. Rev. A* **49**, 2524 (1994).
- [22] T. Ludziejewski, P. Rymuza, Z. Sujkowski, B. Boschung, J.-Cl. Dousse, B. Galley, Z. Halabuka, Ch. Herren, J. Hoszowska, J. Kern, Ch. Rhême, and M. Polasik, *Phys. Rev. A* **52**, 2791 (1995).
- [23] B. Boschung, M. W. Carlen, J.-Cl. Dousse, B. Galley, Ch. Herren, J. Hoszowska, J. Kern, Ch. Rhême, T. Ludziejewski, P. Rymuza, Z. Sujkowski, and Z. Halabuka, *Phys. Rev. A* **52**, 3889 (1995).
- [24] M. Gryziński, *Phys. Rev.* **138**, A336 (1965).
- [25] K.-H. Schratner, in *The Physics of Electronic and Atomic Collisions*, edited by A. Dalgarno, R. S. Freund, P. M. Koch, M. S. Lubell, and T. B. Lucatorto, AIP Conf. Proc. No. 205 (AIP, New York, 1989), p. 215.
- [26] E. D. Donets and V. P. Ovsyannikov, *Sov. Phys. JETP* **53**, 466 (1981).
- [27] T. A. Carlson, W. E. Moddeman, and M. O. Krause, *Phys. Rev. A* **1**, 1406 (1970).
- [28] M. O. Krause, F. A. Stevie, L. J. Levis, T. A. Carlson, and W. E. Moddemann, *Phys. Lett.* **31A**, 81 (1970).
- [29] N. Stolterfoht, H. Gebler, and U. Leithäuser, *Phys. Lett.* **45A**, 351 (1973).
- [30] W. Löw, H. Genz, A. Richter, and K. G. Dyall, *Phys. Lett. A* **100**, 130 (1984).
- [31] G. L. Borchert, W. Scheck, and O. W. B. Schult, *Nucl. Instrum. Methods* **124**, 107 (1975).
- [32] G. L. Borchert, J. Bojowald, A. Ercan, H. Labus, Th. Rose, and O. W. B. Schult, *Nucl. Instrum. Methods Phys. Res. Sect. A* **245**, 393 (1986).
- [33] E. Storm and I. Israel, *Nucl. Data Tables* **7**, 565 (1970).
- [34] K. G. Dyall, I. P. Grant, C. T. Johnson, F. A. Parpia, and E. P. Plummer, *Comput. Phys. Commun.* **55**, 425 (1989).
- [35] M. Polasik, *Phys. Rev. A* **52**, 227 (1995).
- [36] T. A. Carlson, C. W. Nestor, T. C. Tucker, and F. B. Malik, *Phys. Rev.* **169**, 27 (1968).
- [37] T. Mukoyama and K. Taniguchi, *Phys. Rev. A* **36**, 693 (1987).
- [38] T. A. Carlson and C. W. Nestor, *Phys. Rev. A* **8**, 2887 (1973).
- [39] T. A. Carlson, W. E. Moddemann, and M. O. Krause, *Phys. Rev. A* **1**, 1406 (1970).
- [40] J. H. Scofield, *At. Data Nucl. Data Tables* **14**, 121 (1974).
- [41] J. Hoszowska, and J.-Cl. Dousse, *J. Phys. B* (to be published).
- [42] L. Végh and J. Burgörfer, *Phys. Rev. A* **42**, 655 (1990).
- [43] E. G. Berezhko and N. M. Kabachnik, *J. Phys. B* **12**, 2467 (1977).
- [44] V. V. Sizov and N. M. Kabachnik, *J. Phys. B* **13**, 1601 (1980).
- [45] H. Deutsch, D. Margreiter, and T. D. Märk, *Z. Phys. D* **29**, 31 (1994).
- [46] W. Lotz, *Z. Phys.* **216**, 243 (1968).
- [47] J. H. McGuire, N. Berrah, R. J. Bartlett, J. A. Samson, J. A. Tanis, C. L. Cocke, and A. S. Schlachter, *J. Phys. B* **28**, 913 (1995).
- [48] J. Ullrich, R. Moshhammer, H. Berg, R. Mann, H. Tawara, R. Dörner, J. Euler, H. Schmidt-Böcking, S. Hagmann, C. L. Cocke, M. Unverzagt, S. Lencinas, and V. Mergel, *Phys. Rev. Lett.* **71**, 1697 (1993).
- [49] J. H. McGuire and J. C. Straton, in *The Physics of Electronic and Atomic Collisions* (Ref. [25]).
- [50] J. H. McGuire, *Phys. Rev. Lett.* **49**, 1153 (1982).
- [51] R. E. Olson, *Phys. Rev. A* **36**, 1519 (1987).